

Fringe Field of a Focusing Quadrupole in the Beam Line of the LCLS Cryomodule

I. Terechkine

Magnetic field generated by a focusing quadrupole installed in the beam line of the LCLS cryomodule can lead to degradation of the nearest high-Q accelerating cavity as a result of cavity quenching in the external field of the powered quadrupole or after cooling down in the remnant field of the “warm” steel flux return or magnetized parts of the magnetic shields installed inside the cryomodule.

To evaluate these direct and secondary impacts of the magnetic system installed in the cryomodule on its performance, the magnetic field of the system, including the fringe field, must be calculated in the environment of the cryomodule. This note summarizes results of the fringe field modeling.

I. May 2014 shield configuration

Figures 1 and 2 show the part of the LCLS cryomodule on the end with the focusing quadrupole. Configuration of the shield corresponds here to the cryomodule design version of May 2014.

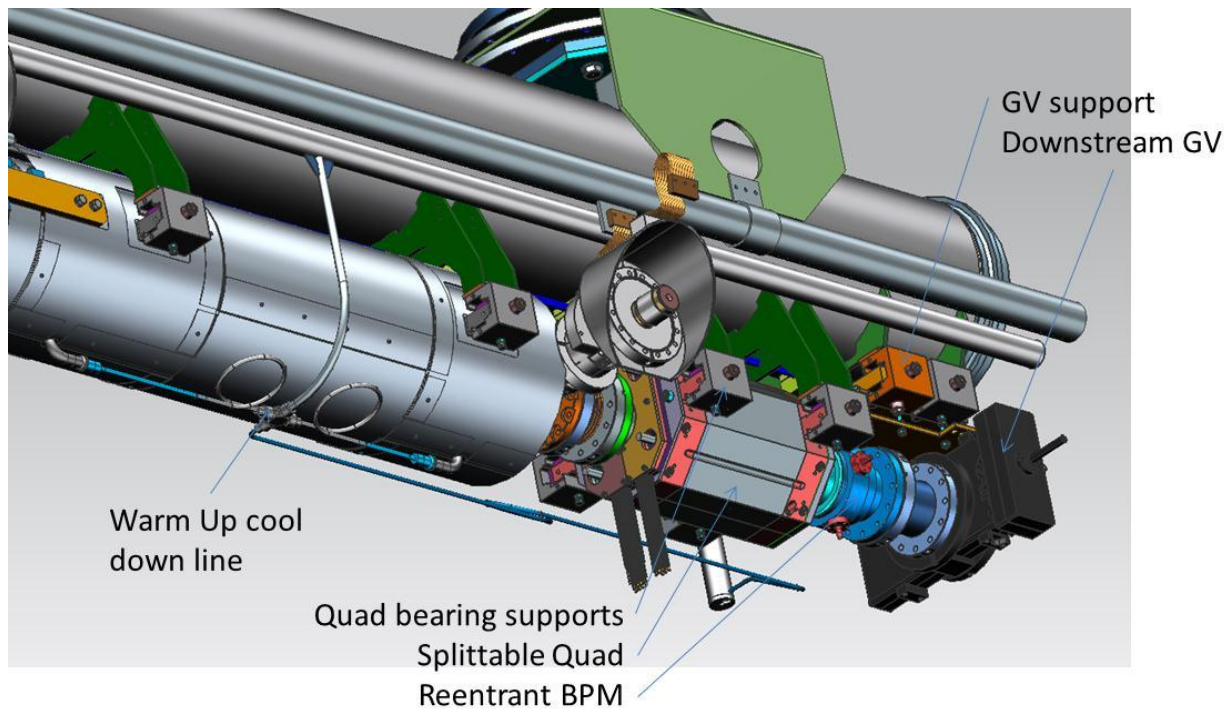


Fig. 1. Elements of the beam line in the LCLS cryomodule.

Distance from the central plane of the quadrupole to the end of the local magnetic shield of the cavity (Cryoperm-10) is ~ 407 mm. The radius of this shield is 220 mm, and the permeability

of the material $\mu = 9000$ was accepted during the modeling. The role of the global magnetic shield in the design is accepted by the material of the vacuum vessel. During this modeling, the inner surface of the vacuum vessel is used as a boundary ($R = 500$ mm) with the perfect magnetic conductor boundary condition. The vertical position of the beam line is shifted down relative to the axis of the vessel by 247 mm.

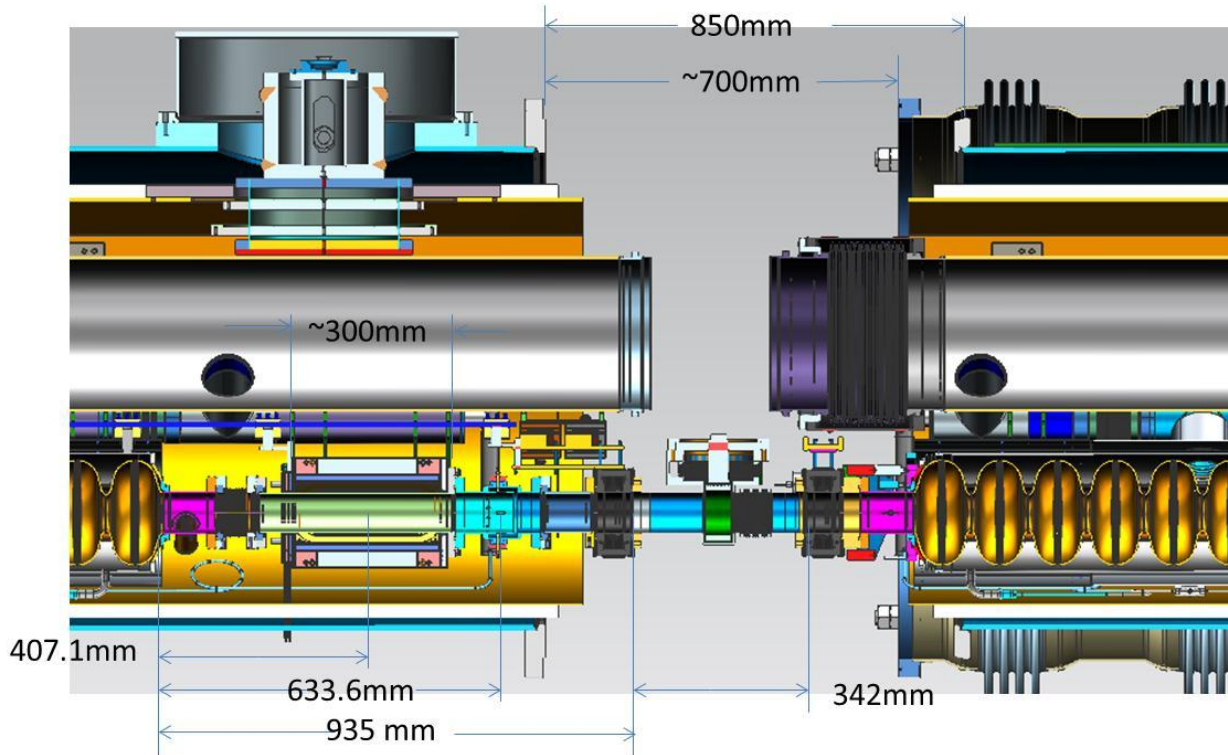


Fig. 2. Relative position of the beam line elements in the LCLS cryomodule.

Magnetic design of the quadrupole was made by V. Kashikhin. Main parameters of the quad are as following:

Parameter	Value
Magnet physical length (mm)	315
Magnet width/height (mm)	220
Pole tip distance (mm)	90
Peak operating current (A)	50
Integrated gradient, T	1.5
Effective length, mm	200
Peak gradient, T/m	6

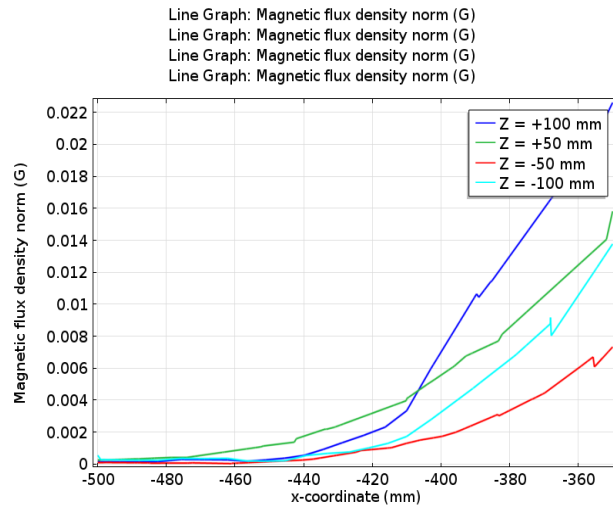


Fig. 5. Field distribution along the lines Z= -50 mm, Z= -100 mm, Z = 50 mm, and Z = 100 mm.

At X = -400 mm, where the first cell starts, the field at Z = 50 mm is ~6 mG, which is just slightly exceeds the specs. The field is within specification in any plane with Z < -405 mm.

2. Field map in the plane perpendicular to the beam line are shown in Fig. 6 for two distances: X = -400 mm (just before the end of the local shield) and X = -450 mm (40mm inside the local shield).

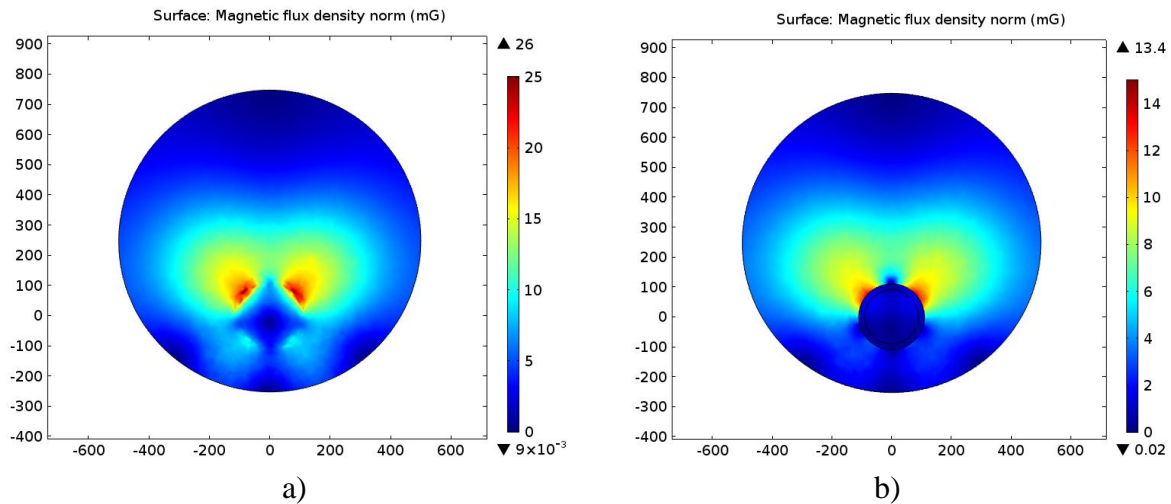


Fig. 6. Field maps in the planes X = -400 mm (a) and X = -450 mm (b)

The field maps agree well with what is shown in Fig. 5.

3. Field maps in the sections where one expects the maximum fringe magnetic field at the location of the global shield are shown in Fig. 7 (X = 0) and Fig. 8 (X = -100 mm). Graphs in the figures show the field distribution along the vertical lines in the planes that start at the global shield (Z = -245 mm) and end on the outer surface of the flux return (Z = -120 mm).

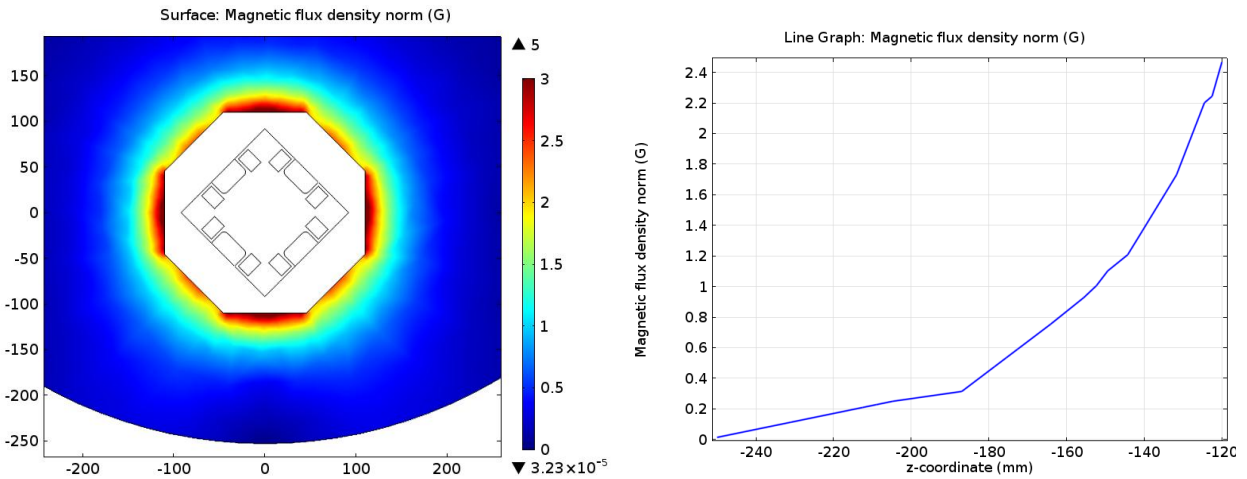


Fig. 7. Field map in the plane $X = 0$ and along the vertical line in this plane between the global shield and the flux return.

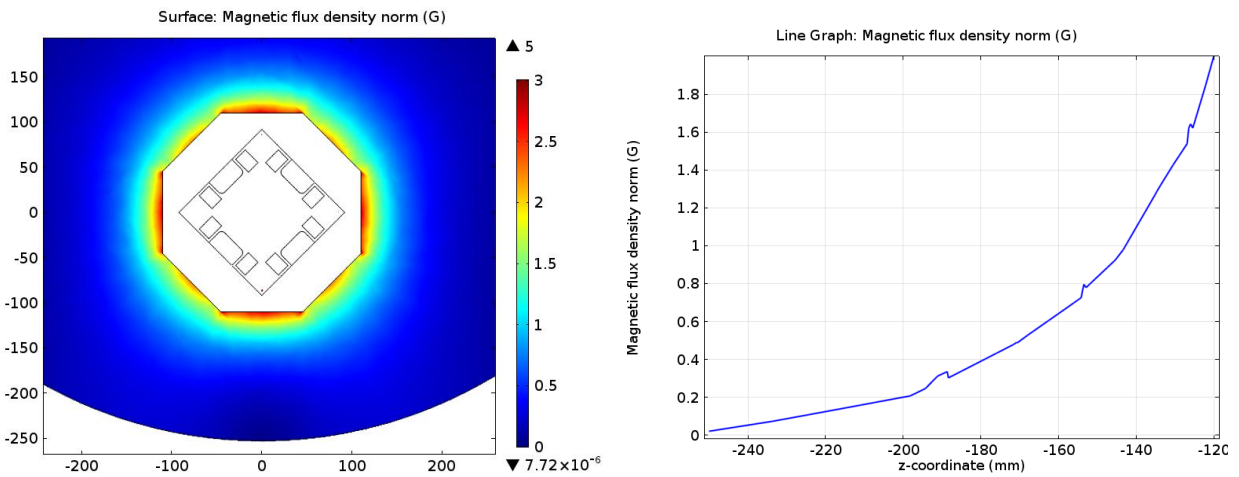


Fig. 8. Field map in the plane $X = -100$ mm and along the vertical line in this plane between the global shield and the flux return.

The field along the surface of the vessel is on the level of ~ 20 mG under the quadrupole and becomes even smaller as one goes farther from the center; it is ~ 5 mG at $X = -250$ mm.

Having in mind this small field, we can conclude that for the May 2014 shield configuration option no danger of steel vessel magnetization exists that comes from the quadrupole.

II. October 2014 shield configuration

In summer 2014, another configuration of the magnetic shield was proposed; it was protruded by ~160 mm towards the quadrupole to fully cover the flange of the cavity. The end diaphragm of the shield has now inner radius $R = 52$ mm. The proximity of the diagram to the cavity forces making another iteration of the modeling to check on the possibility of the shield material magnetization.

Updated geometry of the shield and position of the quadrupole relative to the vacuum vessel and the cavity is shown in Fig. 9 (compare with Fig. 2).

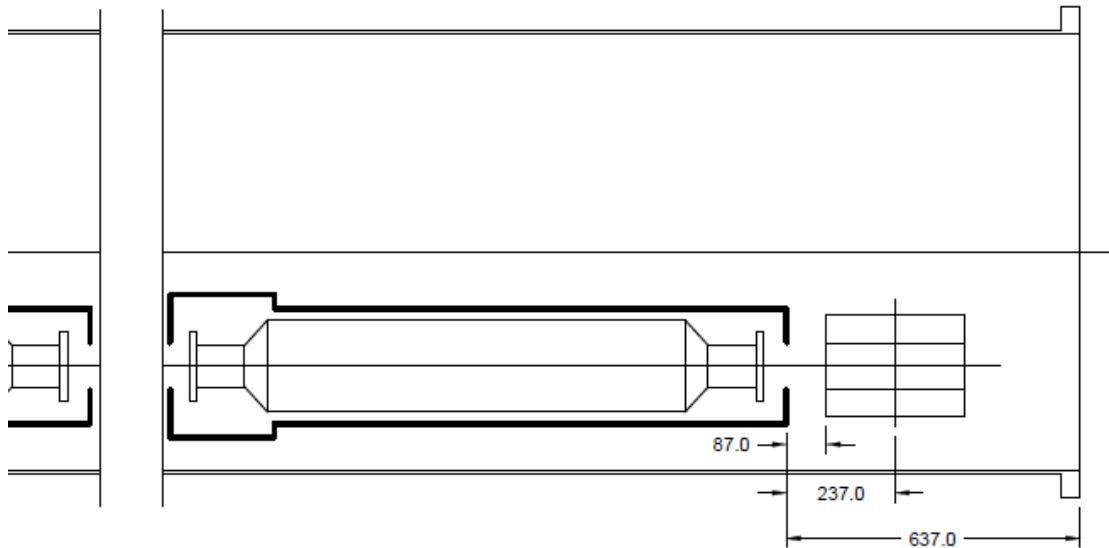


Fig. 9. Position of the quadrupole in the cryovessel relative to the cavity and the magnetic shield.

As a result of closer proximity, the field at the location of the end diaphragm is now greater than it was in the previous case. Fig. 10 shows field map in the plains $X=-245$ and $X=-255$ mm; compare these maps with shown in Fig. 6.

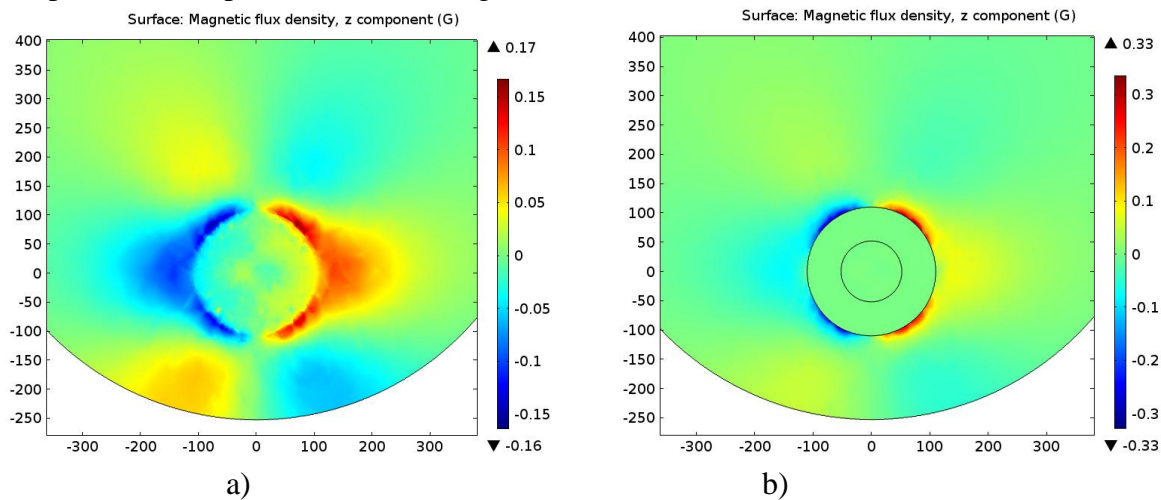


Fig. 10: Field map at $X = -245$ mm (a) and $X = -255$ mm (b)

Magnetic field along the lines: $Z = -100, -50, 0, +50,$ and $+100$ mm from $X = -220$ to $X = -350$ mm is shown in the next plot (Fig. 11): magnetic field inside the shield at the location of the cavity is below 1 mG.

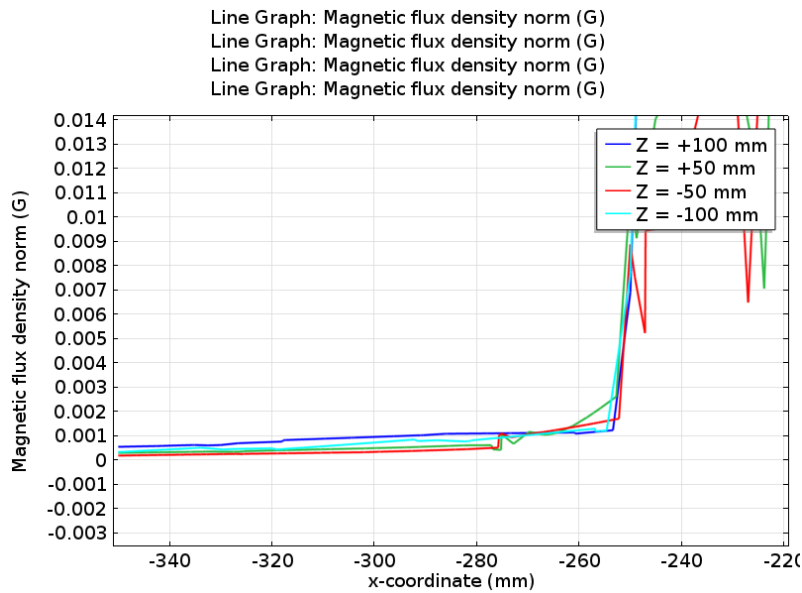


Fig. 11. Field along the lines: $Z = -100, -50, 0, +50,$ and $+100$ mm.

Magnetic field in the vicinity of the quadrupole did not change, and figures 7 and 8 can be used as a reference.

New configuration of the shield still sees very modest magnet field near its surface (less than 500 mG). So, dangerous magnetization of the shield is quite unlikely to happen provided the assembly is made in a properly controlled manner.